Human Settlements Special Issue

MODEL-BASED INTERPRETATION OF HIGH RESOLUTION

SAR IMAGES OF BUILDINGS

Raffaella Guida[a], *Member, IEEE*, Antonio Iodice[a], *Senior Member, IEEE*,

Daniele Riccio[a], *Senior Member, IEEE*, Uwe Stilla[b], *Member, IEEE*

[a]DIET
Università Federico II
Napoli, Italy
{rafguida, iodice, daniele.riccio}@unina.it

[b]Photogrammetry & Remote Sensing
Technische Universität München
Munich, Germany
stilla@tum.de

Abstract

High resolution (HR) Synthetic Aperture Radar (SAR) images of urban areas reveal a large variety of details that, although potentially bringing a lot of information, are often very difficult to interpret. Up to now, most of the research activity in this field has been devoted to the attempt to retrieve geometric information on buildings in terms of their positions and sizes, by using simplified geometrical models. However, this approach does not allow to fully exploit the large amount of information present in HR SAR images. In order to improve information retrieval from such images, and hence their interpretation, in this paper we propose to employ a more refined model that accounts for both geometrical (including fine details) and electromagnetic properties of the building. A meaningful case-study is presented to show that the main features appearing on the SAR image of a building can be interpreted by using our geometric and electromagnetic model. In addition, a first example of retrieval of the complex dielectric constant of building materials from a SAR image is presented.

I. INTRODUCTION

Up today great attention has been posed to extract value added information from Synthetic Aperture Radar (SAR) images of urban areas [1]-[9]. Many different approaches are currently under study but, in most of them, multiple images are employed to exploit either the amplitude [5-6] or the phase information, e.g. [7]. The information extraction appears a fruitful activity: as a matter of fact, urban areas hold many features that seem to be, at least in principle, easily retrievable in a high resolution radar image: shadows or roads appear as dark straight lines separating buildings with canonical shapes [1]; results obtained via qualitative approaches lead to assume that position of the buildings can be estimated [2]. More recently the appearance in SAR images of buildings with simple shapes has been also quantitatively explained [3]-[4],[8]: it has been confirmed that buildings position and dimensions can be retrieved. More specifically, it has been shown that, under appropriate circumstances, the (average) building height can be successfully extracted [3]-[4]. These data are of crucial importance for urban areas monitoring, planning and controlling. Then, in the near future, very interesting results are expected in the field of feature extraction from SAR images of urban areas. According to the user needs, it is supposed that many and different techniques are to be developed and adopted, depending on the scene parameters to be extracted and on the available image spatial resolution.

This paper focuses on future challenges offered by very high resolution SAR amplitude images of urban areas, on their understanding and interpretation, including in the analysis also the shapes of large buildings in the scene; finally, the possibility to quantitatively retrieve the electromagnetic information about the objects that are present in the investigated scene is discussed.

In fact, up to now, most efforts have been done in the attempt to retrieve geometric information from buildings in terms of position [2],[5],[10] and of height, length and width as the sole parameters of their (assumed) simple shape; conversely, research on retrieval of electromagnetic properties is less advanced or mainly limited to the SAR image classification level [1],[10]:

vegetation areas are well separated from built-up areas, roads network is retrieved, but the extraction of dielectric properties of materials is still an open issue.

This can be mostly attributed to the lack of electromagnetic models able to quantitatively describe the interaction of the radar signal with urban areas by taking into account not only the geometry of radar and scene but also the electromagnetic properties of buildings and their surroundings.

As a matter of fact, most of the research on this topic is accomplished by employing some considerations that mainly rely upon the radar acquisition geometry supported by simple models for the buildings shape: this is the case, for instance, of retrieving the building height from the size, on the SAR image, of layover or shadow areas. But, actually, the radar geometry is not sufficient to explain many aspects in SAR images. Moreover, when SAR resolution improves, also new features, often not visible on standard SAR images, become evident thus introducing new troubles in interpretation [12]. And support of High Resolution (HR) SAR images is highly desirable especially for urban planning issues.

In this paper we propose a framework to adopt valuable electromagnetic models and simulation tools for a more detailed investigation and understanding of HR SAR images of urban areas, not restricted to the geometric description. Moreover, we want to assess the reliability of the proposed technique in terms of describing SAR features related to complicate building shapes and electromagnetic parameters: to the scope we select a very meaningful test case that we present and discuss in detail. Incidentally, it is worth recalling that, in the past, use of SAR simulators has been mostly devoted to support the radar and mission design or to test processing algorithms (see, e.g., [13]) but here a SAR raw signal simulator for urban areas [14] is employed to improve interpretation of actual images.

The paper is organized as follows. In Section II we introduce the meaningful test case consisting of one SAR image relevant to an urban area, centred on the Alte Pinakothek in Munich (Germany): this test case shows problems arising in interpretation of high resolution images containing buildings of not simple shapes, emphasizes the need of a model-based quantitative analysis,

provides a support in the presentation of the theoretical framework we propose, and complements our theoretical analysis with experimental data.

In Section III, the radar scattering and SAR image analysis is performed by only considering radar geometry and simple shape models for the building; the limits of such analysis are shown.

Then, a model-based interpretation supported by simulation tools is introduced in Section IV. By means of simulations, consideration of electromagnetic behaviour is shown to be crucial. First steps in quantitative retrieval of dielectric constants are also presented, and the importance of performing analyses based on models is highlighted. The adopted approach is discussed and motivated by comparing simulated and actual SAR images; finally, relevant applications and future perspectives are analyzed in the conclusions.

II. EMPLOYED DATA

Recently, new spaceborne SAR sensors have been launched [15][17]. This radar technology has now reached very high performance, above all in terms of spatial resolution. The spotlight operational mode, in fact, is going to regularly provide SAR images with 1 meter resolution along azimuth and range directions [16]. Till now, similarly very detailed SAR images were only obtained in airborne missions [12] and have never been taken from the space. Hence, in the following, we use airborne HR SAR images.

At a first glance such HR SAR images appear really involved, not only for the well known noise and distortion effects (speckle, shadowing, layover, foreshortening), but also because the different contributions of many objects in the scene, that in previous images were melt together for the low sensors resolution, become now visible and distinct. In HR SAR images of urban areas this appearance is particularly emphasized. In this case, in fact, not only the above mentioned distortions are accentuated for the presence of several buildings close to each other, but in addition these structures let multiple scattering arise which, in turn, produces new features on the SAR image. Moreover, in this kind of scene we find a great variety of objects and materials: big buildings and

little structures, apex and plane roofs, rounded and straight walls, gardens and pavements, concrete or brick surfaces etc.. This wide assortment often produces a very involved HR SAR image and, unfortunately, in most cases a classification of all those structures is carried out in a rough and qualitative way and the interpretation of the image is usually quite poor if compared to the richness of the scenario. Hence, performances of postprocessing algorithms for feature extraction from SAR images are not yet at the level of this technology and many improvements must be brought.

To understand which kind of progress is needed in analysis, understanding and interpretation of HR SAR images of urban areas we inspect and study a meaningful test case.

An optical aerial view of our test area TUM, of 600 m x 400 m, is shown in Fig.1. It is located in the center of Munich (Germany) and presents the group of buildings of the Technische Universität München (TUM) (in the center) and the Alte Pinakothek (at the right bottom) close to the district of Schwabing. Some other buildings and structures of different shapes and materials are dislocated all around.

For each building the interaction with the radar signal is different and, moreover, there is also an electromagnetic mutual interaction among these structures when the scene is hit by the transmitted field. All this affects the corresponding SAR image shown in Fig.2. It is a byte-scaled version of the original SAR image in X-band acquired by the DLR E-SAR sensor during an airborne flight campaign in which the radar functioning mode parameters have been set to achieve high spatial resolution, see Table I. The radar flight trajectory is aligned with the left side of the image.

This SAR image can be analyzed in different ways. Being our aim not to qualitatively classifying the SAR image, but contributing to its interpretation from a quantitative point of view instead, we focus our attention on a relevant structure in the scene trying to retrieve features that cannot be extracted with existing approaches. Hence, our analysis is focused on the building of the "Alte Pinakothek" ("Old Art Gallery") and the surrounding garden, indicated by an arrow in Fig.2.

Generally speaking, the presence of many effects in the SAR images is expected by also employing existing approaches. For example, when the radar flight trajectory and look angle are known we can

foresee the presence of shadows and their direction. In a similar way, it is possible to foresee layover effects for all vertical surfaces, obviously numerous, in an urban scene. And, in fact, such effects are evident in the SAR image of Fig.2. But not everything can be predicted or interpreted by the only knowledge of SAR geometry and assuming a simple shape for the building.

Let us consider the structure of the Alte Pinakothek. A better aerial view of this building is given in Figure 3. It is quite evident that its structure exhibits a symmetric footprint.

On the corresponding SAR image, see Fig.2, the usual sequence of stripes with different brightness is visible, and this can be explained, at least in part, by considering the building geometry, as detailed in the next Section. But there is also an additional interesting feature that is only in part related to the building geometry: the bright stripe corresponding to the south-west wall is brighter on its right part, where some aligned, even brighter, points can be noticed. Such a difference is not visible on optical images, and can not be explained only by the difference in the wall geometry, which is almost the same in both parts of the wall. It is clear that this feature can only be explained by using an electromagnetic model that takes into account the electromagnetic properties of the building materials. This interpretation will be carried out in Section IV.

III. INTERPRETATION FROM IMAGE GEOMETRY

In order to try to understand and interpret some of the effects appearing in the SAR image of the "Alte Pinakothek", geometrical properties of the scene connected to the radar geometry must be considered. We want to show that geometry is not sufficient to explain everything but it is certainly necessary to localize every contribution and to evaluate their relative distances.

Let us analyse the "Alte Pinakothek". For the sake of simplicity, we are not here interested in studying every part of this building but only its central body whose section is represented in Figure 4 where proportions are saved. In the same figure, a grey level representation of the signal backscattered to a SAR sensor is reported; the sensor is supposed to fly perpendicularly to the plane of the picture, which means that longest building walls are parallel to the radar flight trajectory.

This is not the case of the SAR image in Fig.2, but a generalization to a more complicated geometry can be immediately obtained for any flight orientation.

Let us look at Figure 4 and, based on it, analyse which contributions we expect to find in the corresponding SAR image. From left to right (i.e., from near to far range) we expect to find: a layover area; a double reflection line due to the dihedral configuration formed by the building wall with the ground; the backscattering contribution from the apex roof and shadowing. But, if we consider a high resolution image, we expect that each of those areas is not homogeneous. For example, in the layover area the backscattering from the apex roof which presents different inclinations, affects in two different ways the radar signal; in addition, a weak double reflection line should also be expected because of parts of the roof forming a dihedral configuration.

The other contributions can be similarly discussed: after the strong double reflection line, a not homogeneous area of backscattering from roof follows, in which a narrow shadowed area also falls before the larger one.

But this classification of scattering contributions, even if quite detailed, is not sufficient to fully explain the SAR image in Figure 2 and enlarged in Figure 5.

In fact, according to the previous considerations, we would expect to find one strong double bounce line and, perhaps, a weak one, depending on the resolution. However, these two lines should measure the same length. We find out instead that three brilliant lines are present in the SAR image in correspondence of the "Alte Pinakothek" aligned to its greater dimension (lines A, B, C in Fig.5). The second one, line B, might seem shorter, but grey level measures on the SAR image itself reveal that the line has the same length of the others, but is composed of two parts with different scattering amplitudes.

In order to understand which parts of the building give rise to the different bright lines, let us consider the more realistic situation of non-null orientation angle.

First of all, the wall orientation φ with respect to the radar flight trajectory, must be computed, see Fig.5:

$\varphi =\text{tg}^{-1}(y/x)=56.30°$

with

y=number of ground range pixels*ground range pixel spacing=44*0.749269 m=32.97 m

x= number of azimuth pixels*azimuth pixel spacing=15*1.465690 m=21.99 m.

Then, the formulas listed in Table II, based on simple geometrical considerations (see Fig.6), are used to compute the expected ground range distances between the double bounce line and other points of interest indicated in Fig.6: they are reported (in meters and in number of ground pixels) in Table III. These distances are then compared to the ground range size of the entire contribution of the "Alte Pinakothek" (from the first brilliant line to the end of shadowing) and to the distances among the luminous lines, measured on the SAR image: they are reported in Table IV. In Table II, the orientation φ_t is the angle for which the segment c in Figure 6 becomes zero. For $\varphi > \varphi_t$, lines "1" and "2", the former corresponding to the scattering from the top of the building and the latter from the base (where double reflection can be localized), respectively, flip.

Comparing the second row of Table IV with the first column of Table III we can conclude that the measured distances correspond to the segment d, f_φ and s of Fig.6. In fact, differences (see Table V) are of the order of ground range resolution (2.43m), and are compatible with a small error on φ, because an error on θ would have meant errors of different signum for d and s, while they show the same signum, see Table V.

Above analysis leads to the following results: the brilliant lines A, B and C on the SAR image of Fig.5 correspond to the first top border of the building (line "0" of Fig.6), to the double reflection (line "2" of Fig.6) and to the last top border (line "3" of Fig.6), respectively. Anyway, although the appearance of line "2" is easily explained by double bounce reflection, the origin of lines "0" and "3" is not clear: they may arise perhaps from border diffraction, but this cannot be explained on a purely geometrical basis. In addition, line "2" is expected to be meanly uniform while it is not: this is better emphasized in the image cuts of Figs.7-8. Therefore, it is evident that geometry is no more

sufficient to explain some observed SAR image features. An electromagnetic model, also accounting for the materials in the scene, is strongly needed and is adopted in the next section.

IV. MODEL-BASED INTERPRETATION

In this section we propose to improve our interpretation of HR SAR images of urban areas by means of a model based approach supported by appropriate simulation tools. Our goal is to show the importance of analyses based on models and the possibility to quantitatively retrieve, in this way, information about the materials in the scene. In other words this means considering the information on electromagnetic behaviour of materials or, more precisely, on their (complex) dielectric constants.

To this aim, we adopt the geometric and electromagnetic models of scattering from isolated buildings introduced in [18]. These models have been already adopted for developing a SAR raw signal simulator for urban areas [14], which is an efficient simulator based on a frequency domain approach employing Fast Fourier Transforms (FFT) codes.

In Ref.[18], different expressions for the various scattering contributions by a building, under different approximations, are provided. For instance, when the Kirchhoff Approach with the Geometric Optics solution is a good approximation for representing the signal backscattered to the sensor, the double reflection contribution to the radar cross section σ^o is given by the expression below:

$$\sigma^\circ = \frac{\left|S_{pq}\right|^2 hl \tan \vartheta \cos \varphi \left(1 + \tan^2 \vartheta \sin^2 \varphi\right)}{8\pi^2 \cos^2 \vartheta \cdot \sigma^2 \left(2/L^2\right) \cdot \exp\left[\dfrac{\tan^2 \vartheta \sin^2 \varphi}{2\sigma^2 \left(2/L^2\right)}\right]} \quad , \tag{1}$$

where S_{pq} is the generic element of scattering matrix, with p and q each standing for h or v (horizontal or vertical polarization), h and l are building height and length, ϑ is the radar look angle (complementary of the depression angle δ), φ is the wall orientation, σ and L are standard deviation and correlation length of the stochastic process describing the soil roughness, respectively. In S_{pq} the electromagnetic behaviour of surfaces causing the double bounce of the signal, i.e., the building frontal wall and the rough soil, is considered through the dielectric constants of their own materials. In this way, for double reflection as well as for single and triple scattering, we can compute the different radar returns of grass, bricks, concrete, asphalt etc..

Actually, the above mentioned models have been already employed for the retrieval of one key geometric parameter (the building height) from a radiometric one (contribution of double bounce to the radar cross section). This method has been first tested on simulated SAR images [3] and then recently verified on an actual SAR image leading to very promising results [4].

Here we show that the same approach can reveal, and then allow to retrieve, also electromagnetic information from radiometric parameters.

The simulator inputs are [14]: a digital elevation model (DEM) of the scene, electromagnetic and roughness parameters of scattering surfaces, and SAR sensor parameters. As for the DEM, LIDAR data available on the test area have been used and the relevant surface profile is shown in Fig.9. An area of 600 x 400 meters is represented with 1 meter resolution in the horizontal axes directions and 0.2 meter resolution in the altitude profile. The "Alte Pinakothek" is clearly distinguishable.

With regard to the input SAR sensor data, E-SAR radar parameters have been set, corresponding to a single-look image resolutions of 0.27 m and 2.33 m for the azimuth and the ground range, respectively. After processing the SAR raw signal, a multilook has been applied along the azimuth direction leading to a final resolution of 2.18 m x 2.33 m.

With regard to electromagnetic and roughness input parameters, to further stress the considerations of previous section a first simulation has been realized only to highlight the effects caused on the SAR image by the geometric properties of the buildings in the scene. It means that no difference in

materials has been considered, i.e. the same dielectric constant and roughness has been assumed for all the objects in the scene. Moreover, in this first step, we consider only contributions of the first order (i.e., single bounce) to the radar cross section.

The resulting simulated SAR image is shown in Fig.10. Obviously, this image shows only some effects expected for this area. In fact, accounting only for first order contributions to the radar cross section means that only single scattering is represented and, consequently, only layover and shadow areas are clearly visible. Instead, looking at the actual SAR image in Fig.2 or Fig.5, we note different brilliant lines that have not been represented in the simulation in Fig.10.

In order to consider also higher order contributions (i.e., multiple bounces), arising from dihedral and trihedral configurations formed by a building with the soil on which it is placed and the other structures nearby, we have to use the full electromagnetic model of [14],[18]. However, to maintain simulation efficiency and low computational costs, we assume a simplified geometrical model for the building (in practice an isolated parallelepiped on a rough terrain). In our case, being interested in the first and second order contributions produced by the main wall, we assumed the same height for all the points of the roof (20 m) thus disregarding the presence of a roof slope. In this way, in spite of the geometry simplification, we can more satisfactorily explain some effects in the actual SAR image. In fact, we can now represent in the simulated SAR image also contributions of second and third order (higher order contributions do not arise for the geometric model adopted).

Indeed, triple scattering, even if accounted for, is not clearly visible both in real and simulated images because it produces too weak radar return.

Double reflection, instead, is of great interest and its representation on simulated SAR images is helpful for a better interpretation of real SAR images. As a matter of fact, this contribution brings an important information content which, if retrieved, can be used for supporting image analysis.

Even if not all necessary information is available, our models and simulation tools can support human interpretation of SAR image in the following way.

Let us look again at image in Fig.5. We have already realized and discussed some unexpected effects. We aim now to get the causes of this appearance. A certain ground truth is known about that area; in particular, buildings dimensions are given. Such information relevant to the art gallery reveals that the structure is perfectly symmetric. Moreover, the garden surrounding the building is symmetric with respect to an axis perpendicular to the large frontal wall and passing through its center. In these conditions, should we consider only geometric properties of the strucutures, we could never explain the effect appearing in the SAR image: a geometrically symmetric structure presents a not radiometrically symmetric strip of double reflection. Looking at the parameters appearing in Eq.(1) we can find an explanation of this effect.

We know, by the ground truth, that the building is symmetric. Consequently, we expect that each section has the same height h. The garden in front of the wall is mainly constituted by grass for which the same roughness, in a statistical sense, can be assumed for all its extension. This implies that the same couple of roughness parameters (σ, L) should be adopted for computing the intensity of double bounce. Moreover, the radar look angle θ is the same for all the acquisition time (and so for each subarea in the image) and, obviously, each part of the same wall presents the same orientation φ with respect to the radar flight trajectory. But Eq.(1) takes into account also the electromagnetic behaviour of the involved materials. Having the wall the same ground in front of it (mainly grass), see Fig.3, there is only one way to explain the effect shown by the SAR image: the east and the west side of the wall present different dielectric constants, i.e., they are made of different materials.

This conclusion has been reached by only using the SAR image, the scattering model and the DEM of the area. No further ground truth was needed (which is usually not available in most practical cases). In the case study at hand, the correctness of the above conclusion can be confirmed by a site survey and by available historical information. In fact, the "Alte Pinakothek", built in 1836, was severely bombed during the second world war. But the architect Hans Döllgast, engaged in the '50s for the restoration of the gallery, did not reconstruct the building from the beginning. He used

together some old bricks coming from the ruins and new ones and backed the wall with steel pipes because he thought that the wounds of a war have to remain visible to help people to keep the memory alive. In Fig.11 a picture of the south wall of the Alte Pinakothek is reported. The main door corresponds to the centre of the wall. We note the presence of different materials just where it was expected, that is on the east side.

Now, looking closely at Fig.5, we can number seven sparkling points. Looking again at Fig.11, we number seven steel pipes which can be considered the main cause of the different intensities in the double reflection line.

In order to have further confirmation of the theory above, we first of all compare the distances between each couple of brilliant points on the SAR image to the actual one. Results are reported in Table VI. The error is still smaller than the SAR resolution.

Then we move to a radiometric measure. We evaluate the mean grey value I_{ew} of the part of the double reflection line due to the east part of the wall with the steel pipes and that relevant to the west side, I_{ww}. Their ratio measures $I_{ew}/I_{ww}=3.37$. We now perform different simulations by varying the complex dielectric constant of the east part of the building, as detailed below, and compute the same grey level ratio on the simulated images. This procedure on one hand provides a further confirmation that the proposed image interpretation is correct, and on the other hand represents a first example of application of a method to estimate the complex dielectric constant of the building materials from a SAR image.

We consider again the model proposed in Eq.(1) with all the available data except for the dielectric constant of the material of the pipes that we want to try to retrieve. For the sake of simplicity, an average relative dielectric constant of the wall ε_m has been estimated as a weighted average (according to the percentage of presence) of the relative dielectric constant of the bricks ε_b, of the glass ε_g and of pipe material ε_p. The pipes have a diameter of about 15 cm and are 20 meters high for a coverage area A_p of about 21 m^2. The glass, instead, covers the east side of the wall with an

area A_g of 276 m^2. Finally, the other parts are made of bricks, for an area A_b. The total area A_t of this part of the wall measures 60m x 20m (1200m^2).

Then the mean dielectric constant ε_m of the east part of the wall can be written as:

$$\varepsilon_m=(A_p*\varepsilon_p+A_g*\varepsilon_g+A_b*\varepsilon_b)\ /A_t\ .$$

In our case, it turns out that

$$\varepsilon_m=(21\varepsilon_p+276\varepsilon_g+903\varepsilon_b)\ /1200.$$

It is well known that, for typical building materials (like glass, brick, concrete, limestone, marble) the real part ε' of the relative dielectric constant has a small range of variability (2÷12), cfr. [19-22], while the imaginary part ε'', related to the conductivity, can vary of many orders of magnitude. According to Refs. [19-21], for the real part of the relative permittivity of glass, bricks and steel at 9.6 GHz (frequency of SAR image in Fig.5), the following values have been adopted:

$$\varepsilon'_g=6.2 \qquad \varepsilon'_b=4.5 \qquad \varepsilon'_p=3.1.$$

For the imaginary parts, we suppose to know those of glass and bricks ($\varepsilon''_g=0.037$, $\varepsilon''_b=0.3$, see respectively [19] and [20]) and to retrieve that of pipes ε''_p. A similar mean dielectric constant has been evaluated for the west part of the building, but assuming a coverage made only of glass and bricks: accordingly, the mean dielectric constant of the west part of the wall ε_w has been evaluated as:

$$\varepsilon_w=(276\varepsilon_g+924\varepsilon_b)\ /1200 = 4 - j0.024.$$

We perform different simulations by assuming different values of the imaginary part of the pipe dielectric constant, shown in the second column of Table VII. The corresponding image is shown in Fig.12, and the corresponding values of I_{ew}/I_{ww} measured on the simulated images are listed in the third column of Table VII.

A good agreement with the ratio measured on the real image is obtained for a value of the imaginary part of the dielectric constant equal to 10^7 corresponding, at 9.6 GHz, to a conductivity of $5.34*10^6$ S/m, cfr. [22]. This is in reasonable agreement with conductivity of some metals, and in

particular steel. A simulation of the building with no steel pipes would give an image in which all the wall appears like the right part of the wall in Fig.12.

The obtained results and the future perspectives are commented in the conclusions.

V. CONCLUSIONS

In this paper new challenges have been faced: the detailed interpretation of high resolution SAR images and the quantitative retrieval of dielectric properties of building materials by measuring the relevant high resolution SAR image.

The proposed analysis belongs to the highly valuable set of SAR feature extraction techniques that make use of one single SAR amplitude image, possibly in the azimuth - slant range SAR natural coordinates: development and presentation of these techniques are very complicated because they must apply to a minimum set of remotely sensed data; but working with just one single SAR amplitude image holds very valuable advantages: it does not require intensive use of high resolution operational modes for the SAR sensor; can be applied to a very large amount of acquired data; is, in practice, the sole applicable approach in case of (quasi) real time applications (as required for instance in case of natural disaster), and, last but not least, does not require any sophisticated or time consuming SAR image post-processing (e.g., phase preserving issues, multiple images co-registration, geocoding, etc.).

The presented study has been based on geometrical and electromagnetic models and has been supported by appropriate SAR simulation tools.

To be consistent with actual situations one meaningful test case has been fruitfully considered along the discussion: a SAR image of an urban scene has been analysed in detail introducing both geometric and electromagnetic measures. This approach has allowed a more complete interpretation of the image since some unexpected effects have been very satisfactorily explained. Our image interpretation has been verified by comparison with an innovative ground truth devoted to acquire

not only average geometrical properties of a building, but also relevant geometrical (shape) and electromagnetic (materials constituting the building walls) parameters details. Accordingly, it can be assumed that the main result of this paper relies in having demonstrated the key influence (up to now almost not expected) in HR SAR images of urban areas of these parameters.

The results presented here have mainly considered the mechanism of double reflection, but further and similar analyses can also be led on single scattering (considering, for instance, the brightness of layover which is also affected by the wall materials) and are at moment under study.

The good agreement between measures and simulations encourage further analyses with such a model based approach.

REFERENCES

[1]   F.Dell'Acqua, P.Gamba, "Detection of urban structures in SAR images by robust fuzzy clustering algorithms: the examples of street tracking", *IEEE Trans. Geosc. Remote Sensing*, vol.39, pp.2287-2297, 2001.

[2]   M.Quartulli, M.Datcu, "Stochastic Geometrical Modeling for Built-Up Area Understanding from a Single SAR Intensity Image with Meter Resolution", *IEEE Trans. Geosc. Remote Sensing*, vol.42, pp.1996-2003, 2004.

[3]   R.Guida, G.Franceschetti, A.Iodice, D.Riccio, G.Ruello, "Accuracy of Building Height Estimation from SAR images", *Proceedings of the International Geoscience and Remote Sensing Symposium*, Denver (Colorado, USA), 2006.

[4]   R.Guida, G.Franceschetti, A.Iodice, D.Riccio, G.Ruello, U.Stilla, "Building Feature Extraction via a Deterministic Approach: Application to Real High Resolution SAR Images",

Proceedings of the International Geoscience and Remote Sensing Symposium, Barcelona (Spain), 2007.

[5] R.Bolter, "Reconstruction of Man-Made Objects from High Resolution SAR Images", *IEEE Aerospace Conference Proceedings*, vol.3, pp.287-292, 2000.

[6] D.Perissin, A.Ferretti, "Urban-Target Recognition by Means of Repeated Spaceborne SAR images", *IEEE Trans. Geosc. Remote Sensing*, vol.45, pp.4043-4058, 2007.

[7] C.Tison, F.Tupin, H.Maitre, "A Fusion Scheme for Joint Retrieval of Urban Height Map and Classification from High Resolution Interferometric SAR Images" *IEEE Trans. Geosc. Remote Sensing*, vol.45, pp.496-505, 2007.

[8] A.Thiele,   E.Cadario,   K.Schulz,   U.Thoennessen,   U.Soergel,   "Building Recognition From Multi-Aspect High-Resolution InSAR Data in Urban Areas", *IEEE Trans. Geosc. Remote Sensing*, vol.45, pp.3583-3593, 2007.

[9] U.Stilla, U.Soergel, U.Thoennessen, "Potential and limits of InSAR data for building recon-struction in built up-areas". ISPRS Journal of Photogrammetry and Remote Sensing, vol.58, no.1-2, pp.113-123, 2003.

[10] U.Stilla, U.Soergel, "Reconstruction of buildings in SAR imagery of urban areas", In: Q.Weng, D.A.Quattrochi (eds) Urban Remote Sensing, Taylor & Francis, 47-67, 2006.

[11] U.Stilla, S.Hinz, K.Hedman, B.Wessel B "Road extraction from SAR imagery" In: Q.Weng (ed.) Remote Sensing of Impervious Surfaces. Boca Raton, FL: Taylor & Francis, 179-214, 2007.

[12] U.Stilla, "High resolution radar imaging of urban areas". In: Fritsch D (ed.) Photogrammetric Week 07. Wichmann: Heidelberg, 149-158, 2007.

[13] G.Franceschetti, A.Iodice, S.Maddaluno, D.Riccio, "Effect of Antenna Mast Motion on X-SAR/SRTM Performance", *IEEE Trans. Geosc. Remote Sensing,* vol.38, no.5, pp.2361-2372, 2000.

[14] G.Franceschetti, A.Iodice, D.Riccio, G.Ruello "SAR raw signal simulation for urban structures", *IEEE Trans. Geosc. Remote Sensing*, vol.41, pp.1986-1995, 2003.

[15] S.Ochs, W.Pitz, "The TerraSAR-X and TanDEM-X Satellites", *Proceedings of 3rd International Conference on Recent Advances in Space Technologies*, Istanbul (Turkey), pp.294-298, 2007.

[16] R.Werninghaus, S.Buckreuss, W.Pitz, "TerraSAR-X Mission Status", *Proceedings of the International Geoscience and Remote Sensing Symposium*, Barcelona (Spain), 2007.

[17] P.Lombardo, "A multichannel spaceborne radar for the COSMO-Skymed Satellite Constellation", *Proceedings of Aerospace Conference*, pp.111-119, 2004.

[18] G.Franceschetti, A.Iodice, D.Riccio, "A canonical problem in electromagnetic backscattering from buildings", *IEEE Trans. Geosc. Remote Sensing*, vol.40, pp.1787-1801, 2002.

[19] H.E.Bussey, J.E.Gray, E.C.Bamberger, E.Rushton, G.Russell, B.W. Petley, D.Morris, "International Comparison of Dielectric Measurements", *IEEE Trans. Instrum. Meas.*, vol.13, no.4, pp.305-311,1964.

[20] Ghodgaonkar, D.K.; Varadan, V.V.; Varadan, V.K, "Free-space measurement of complex permittivity and complex permeability of magnetic materials at microwave frequencies", *IEEE Trans. Instrum. Meas.*, vol.39, no.2, pp.387-394,1990.

[21] H.F.Richards, "The Contact Electricity of Solid Dielectrics", *Phys. Rev.*,vol.22, no.2, pp.122-133, 1923.

[22] M.Bingle, D.B.Davidson, J.H.Cloete, "Scattering and absorption by thin metal wires in rectangular waveguide-FDTD simulation and physical experiments", *IEEE Trans. Microwave Theory Tech.*, vol.50, no.6, pp.1621-1627, 2002.

Captions of Tables

Table I – Radar parameters relevant to the multilook (ML) SAR image in Fig.2.

Table II – Expressions for ground range distances among different contributions in the SAR image of the "Alte Pinakothek". For $\varphi= \varphi_t=\cos^{-1}(base/2h_2*\tan\theta)$ the distance c is zero.

Table III – Ground range distances among different contributions in the SAR image of the "Alte Pinakothek" for the retrieved orientation $\varphi=56.30°$.

Table IV – Measured distances among the brilliant lines in the SAR image of the "Alte Pinakothek".

Table V – Comparison between expected and measured distances among the brilliant lines in the SAR image of the "Alte Pinakothek".

Table VI – Measured distances among the seven sparkling points in the double reflection contribution in the east side of the "Alte Pinakothek".

Table VII – Ratios between the measured values of the intensities of the double reflection contribution of the east wall I_{ew} and the west wall I_{ww} for different values of ε''_p.

Table I

Sensor	E-SAR
Radar centre frequency	9.6 GHz
Radar look angle θ	55°
Depression angle δ	35°
Polarization	HH
Azimuth resolution (ML)	3.00m
Slant range resolution (ML)	1.99m
Azimuth pixel spacing	1.46569m
Ground range pixel spacing	0.749269m

Table II

Frontal view (φ=0°)	Lateral view(φ<φ$_t$=48.48°)	Lateral view(φ>φ$_t$=48.48°)
d=h$_1$*tg(δ)=14.00m	d= 14.00m	d=14.00m
f=base-d=26.00-14.00=12.00m	f$_\varphi$=f+(base/cosφ-base)	f$_\varphi$=f+(base/cosφ-base)
c=|h$_2$*tg(δ)-base/2|	c$_\varphi$=|h$_2$*tg(δ)-(base/cos φ)/2|	c$_\varphi$=|h$_2$*tg(δ)-(base/cos φ)/2|
a=d-c	a$_\varphi$=d-c$_\varphi$	a$_\varphi$= d+c$_\varphi$
s=d+ h$_1$*tg(π/2- δ)= =14.00+28.56=42.56m	s= 42.56m	s=42.56m

Table III

Image view ($\varphi=56.30°$)	
[m]	[ground pixels]
d=14.00m	18-19
f_φ=f+(base/cosφ-base)=32.86m	43-44
c_φ=|h_2*tg(δ)-(base/cos φ)/2|=3.82m	5-6
a_φ= d+c=17.82m	23-24
s=42.56m	56-57

Table IV

	Total extension	Distance between the first and second line (from left to right)	Distance between the second and third line (from left to right)	Distance between the third line and the end of shadowing (from left to right)
Ground pixels	110	16	40	54
meters	82.42	11.98	29.97	40.46

Table V

	Expected [m]	Measured [m]	Error [m]
d	14.00	11.98	2.02
f_φ	32.86	29.97	2.89
s	42.56	40.46	2.10

Table VI

Couples of points (from left to right)	Measured distance [m]	Mean distance [m]	Ground truth [m]	Error [m]
1	7.866			
2	7.434			
3	5.367	6.635	5	1.635
4	6.844			
5	6.008			
6	6.288			

Table VII

SAR image	ε''_p	I_{ew}/I_{ww}
Fig.13a	10^3	2.89
Fig.13b	10^5	3.03
Fig.13c	10^7	3.50
Fig.13d	10^8	3.96

Captions of Figures

Figure 1 – Aerial image (Orthophoto) of the test area TUM, the "Alte Pinakothek" is on the right.

Figure 2 – SAR image of the test area TUM in Fig.1, acquired by the sensor E-SAR (DLR-HR).

Figure 3 – Enlarged view of the "Alte Pinakothek".

Figure 4 – Representation of SAR image formation for the main body of the art gallery. The radar flight trajectory is perpendicular to the plane of the picture and parallel to the building wall ($\varphi=0$). First and second order contributions have been considered and represented in slant range-azimuth plane in the top right.

Figure 5 – Enlarged view of the SAR image in Fig.2, the picture gallery is in the center.

Figure 6 – Representation of SAR image formation for the main wall of the picture gallery when $\varphi\neq0$. Here, a simpler distinction of contributions has been made: scattering falling before double reflection, double reflection, scattering falling after double reflection, shadow.(a) $\varphi>\varphi_t$; (b) $\varphi<\varphi_t$.

Figure 7 – Cut in the SAR image along the wall orientation (from west to east): the continuous line is relevant to the double reflection (line n.2 in Fig.6), the discontinuous line is relevant to the single scattering from the first corner (line n.0 in Fig.6).

Figure 8 – Cut in the SAR image along the wall orientation (from west to east): the continuous line is relevant to the double reflection (line n.2 in Fig.6), the discontinuous line is relevant to the single scattering from the last corner (line n.3 in Fig.6).

Figure 9 – 3D view of LiDAR data mapping the test area TUM (see Fig.1) (axes are labelled in meter).

Figure 10 – Simulated SAR image using LiDAR data of test area TUM.

Figure 11 – South wall of the "Alte Pinakothek".

Figure 12 – Simulated SAR image of the Alte Pinakothek with E-SAR sensor parameters for $\varepsilon''_p=10^7$, $\sigma=5.34*10^6$ S/m. Near range is on the left. Other simulated images have similar appearance.
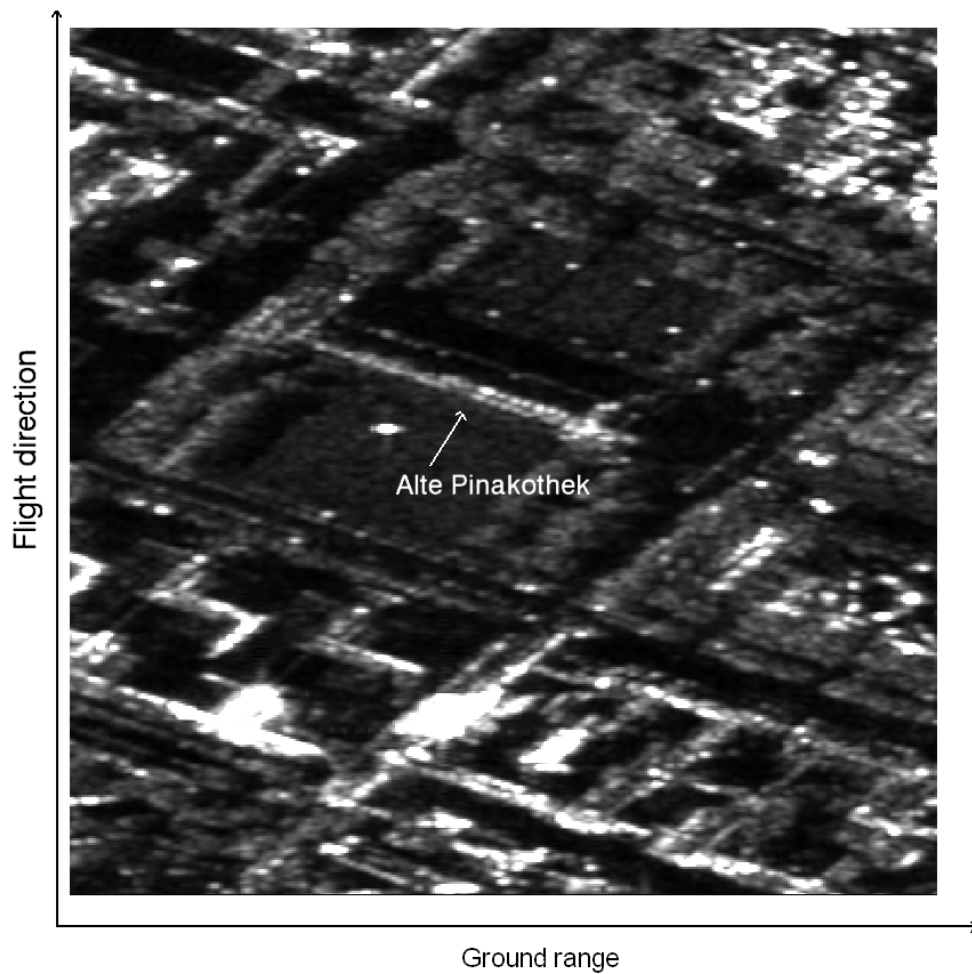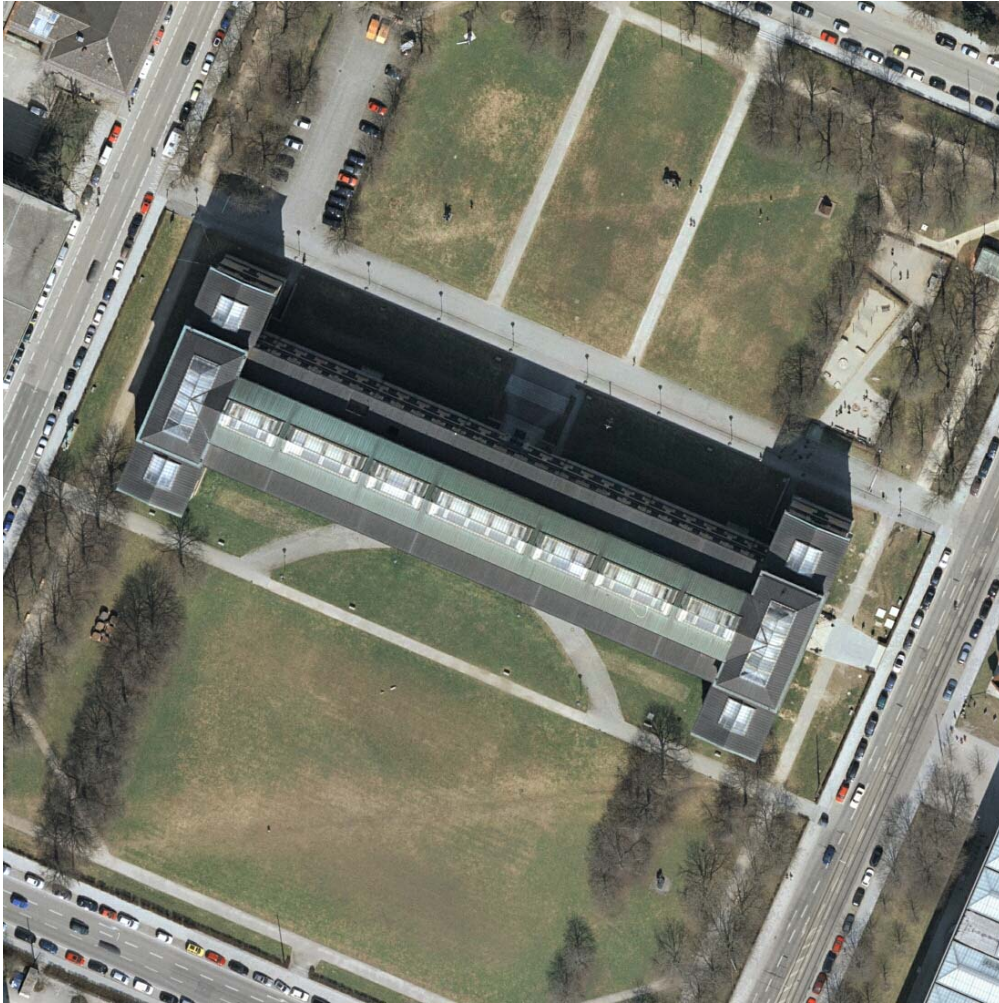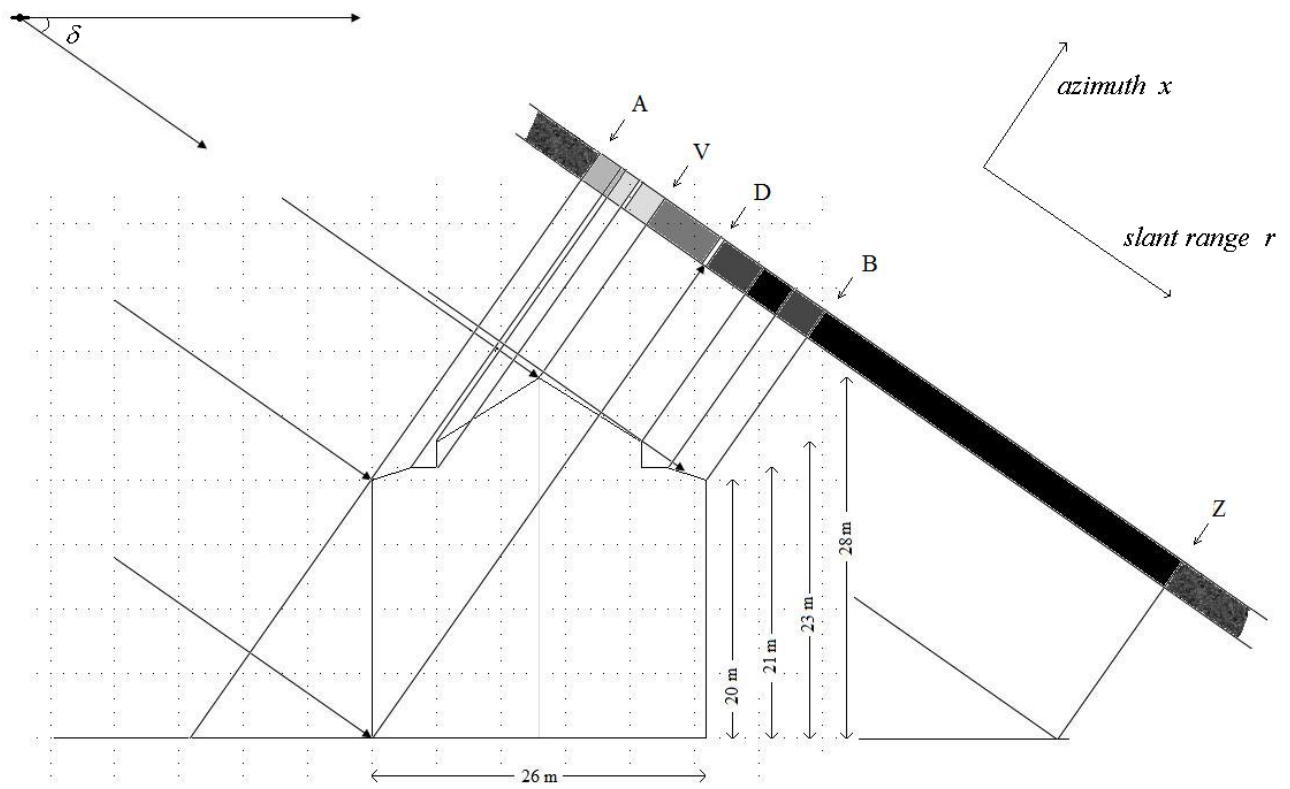
Figure 1

Figure 2

Figure 3

A=slant range localization
   of the backscattering
   from the first corner

V=slant range localization
   of the backscattering
   from the top

D=slant range localization
   of the double reflection line

B=slant range localization
   of the backscattering
   from the last corner

AD=slant range extension
    of layover

DB=slant range extension
    of the backscattering
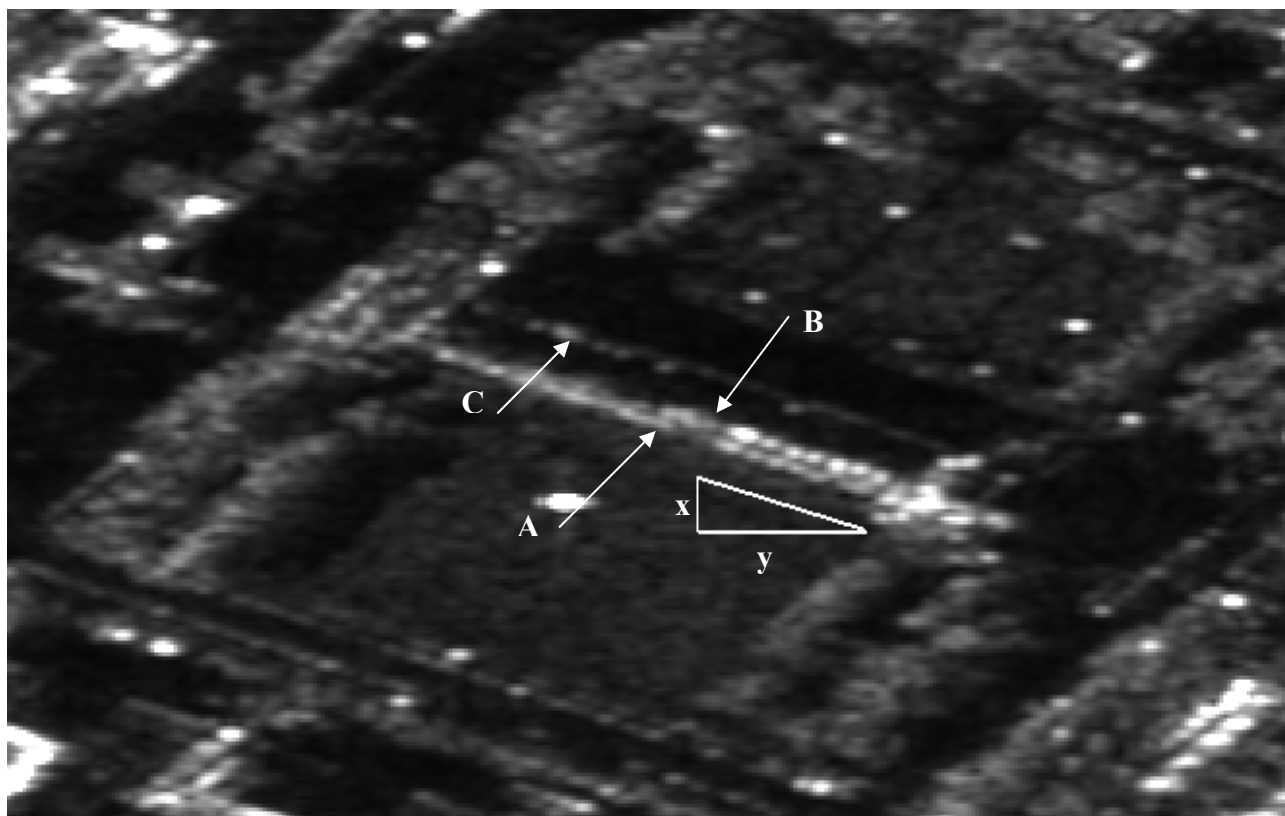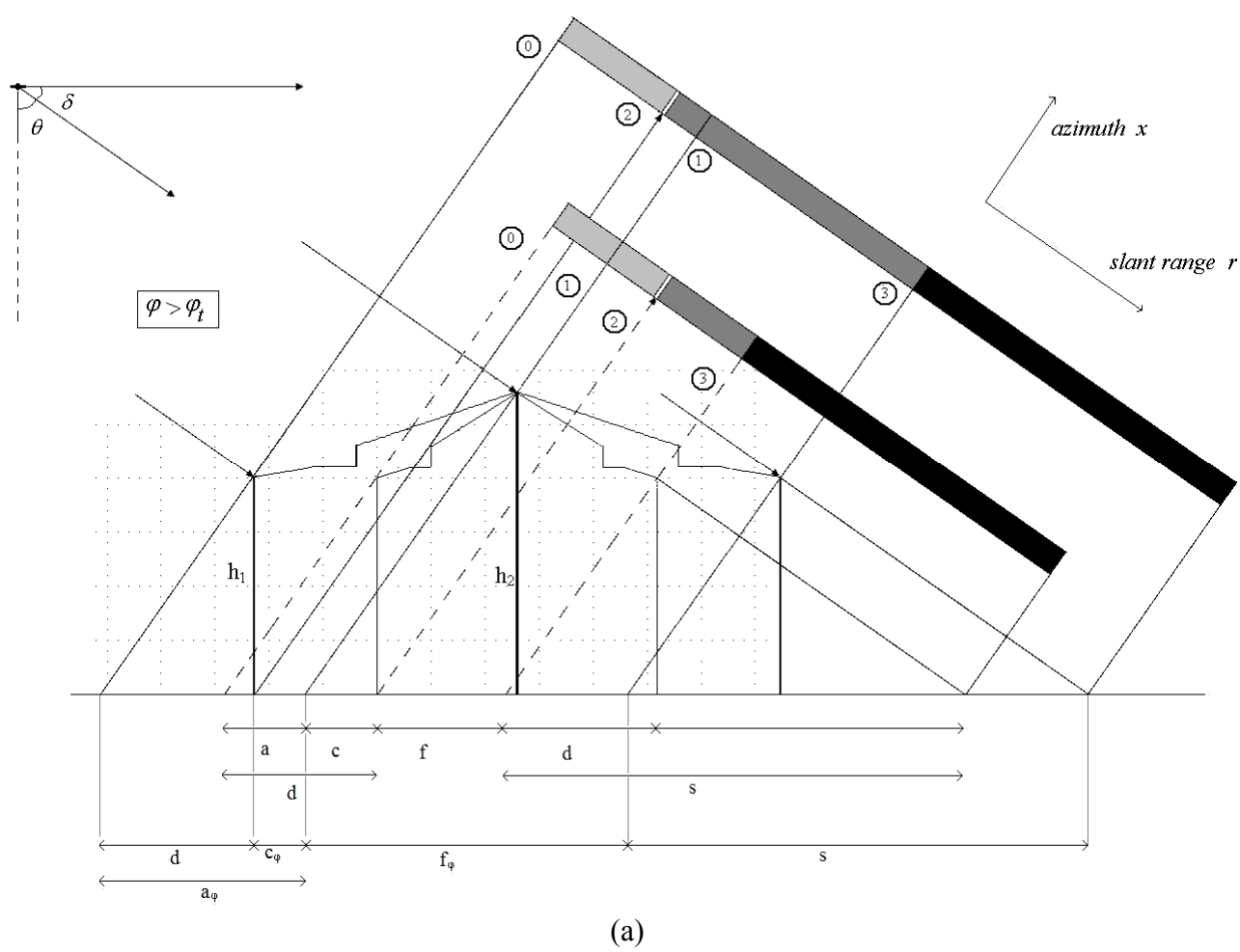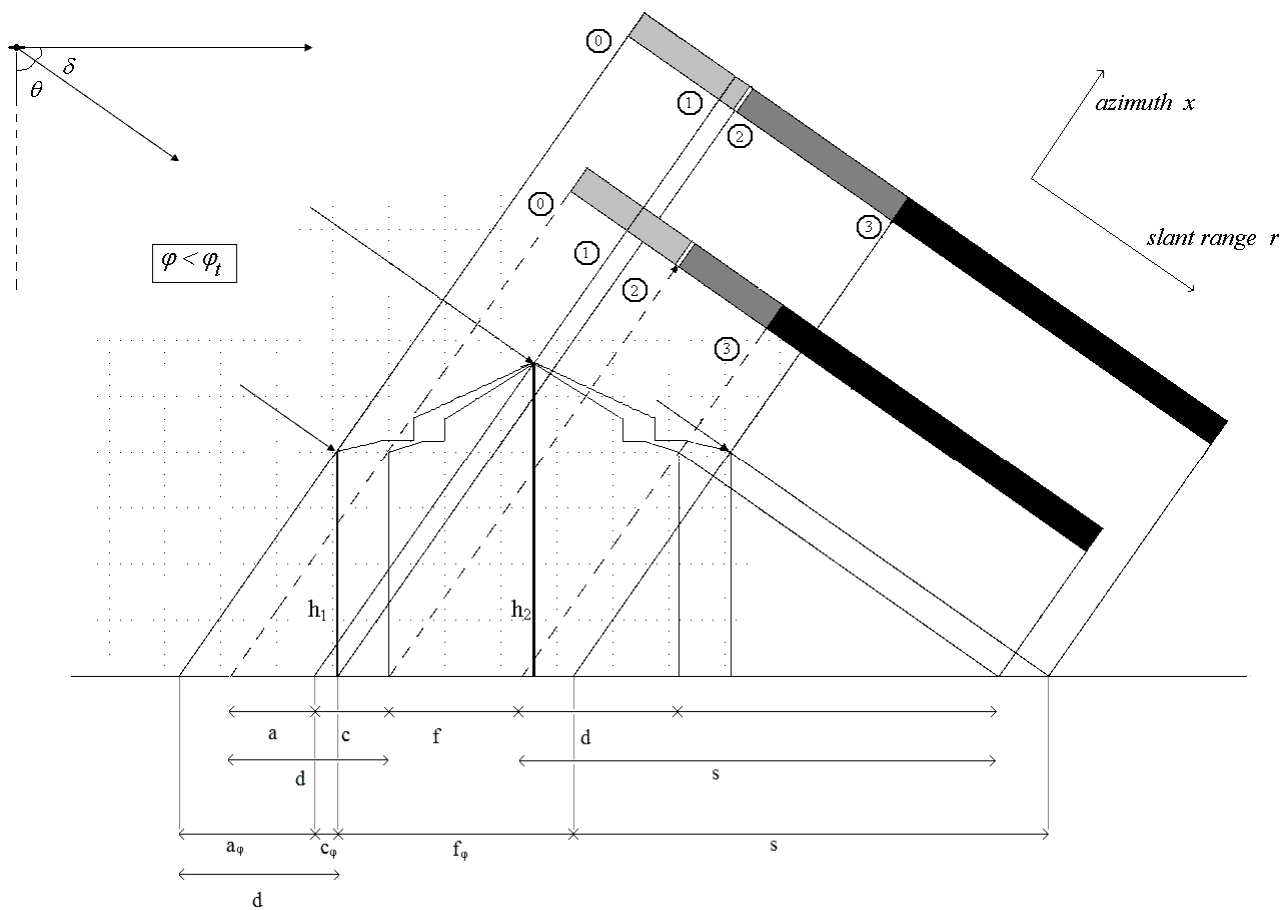   from the roof

BZ=slant range extension
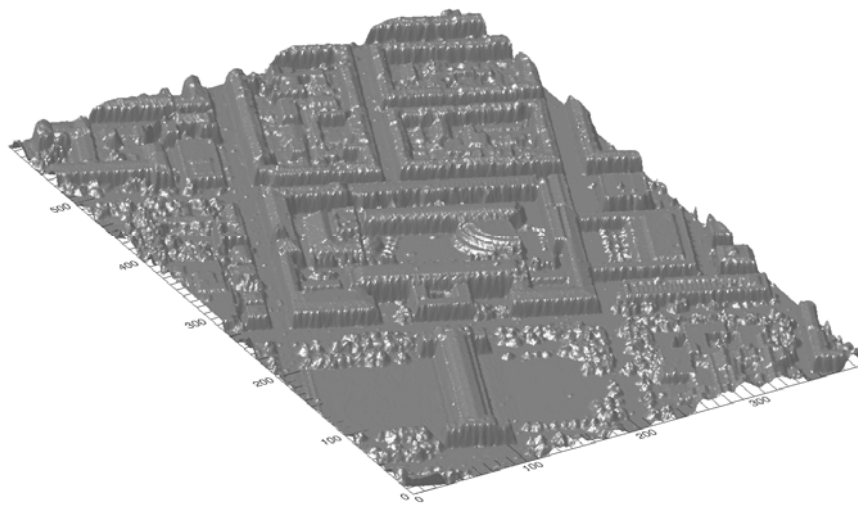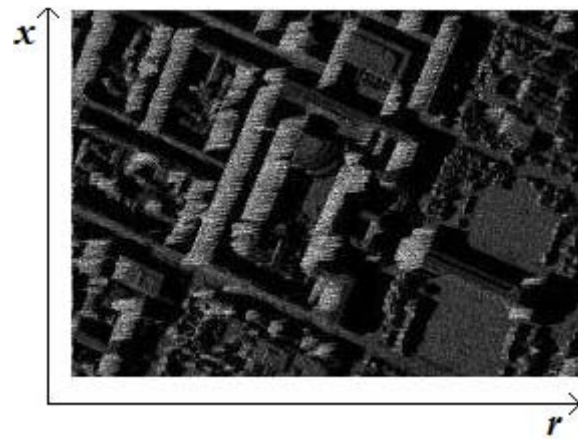   of shadow

Figure 4

Figure 5

(a)

(b)
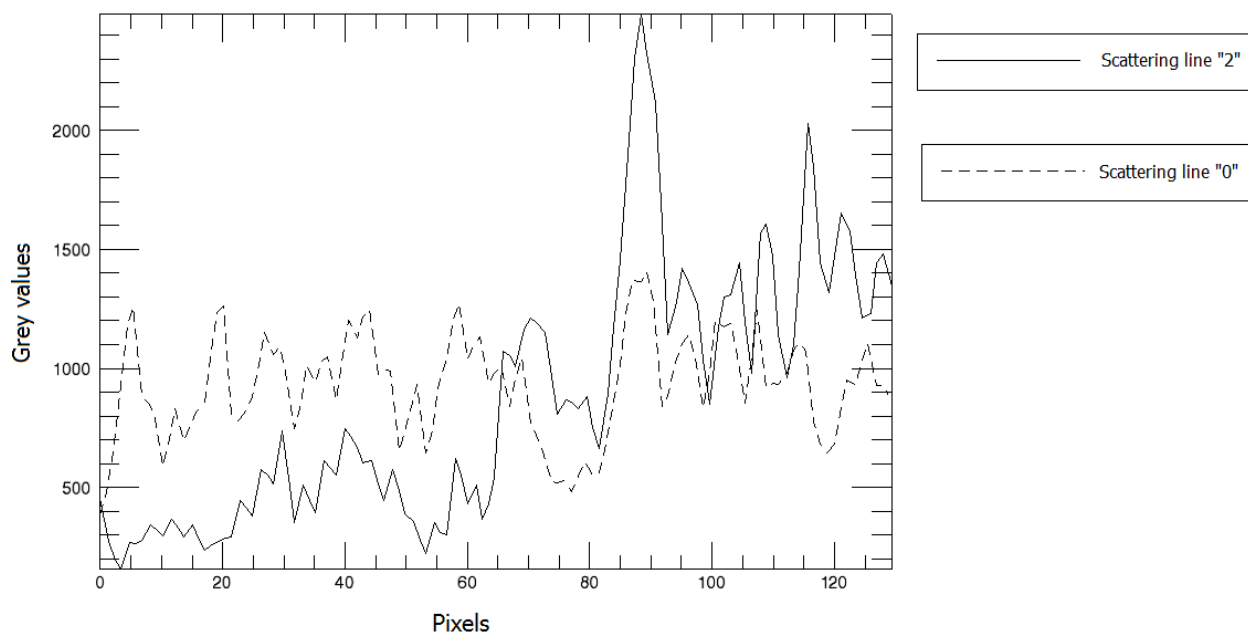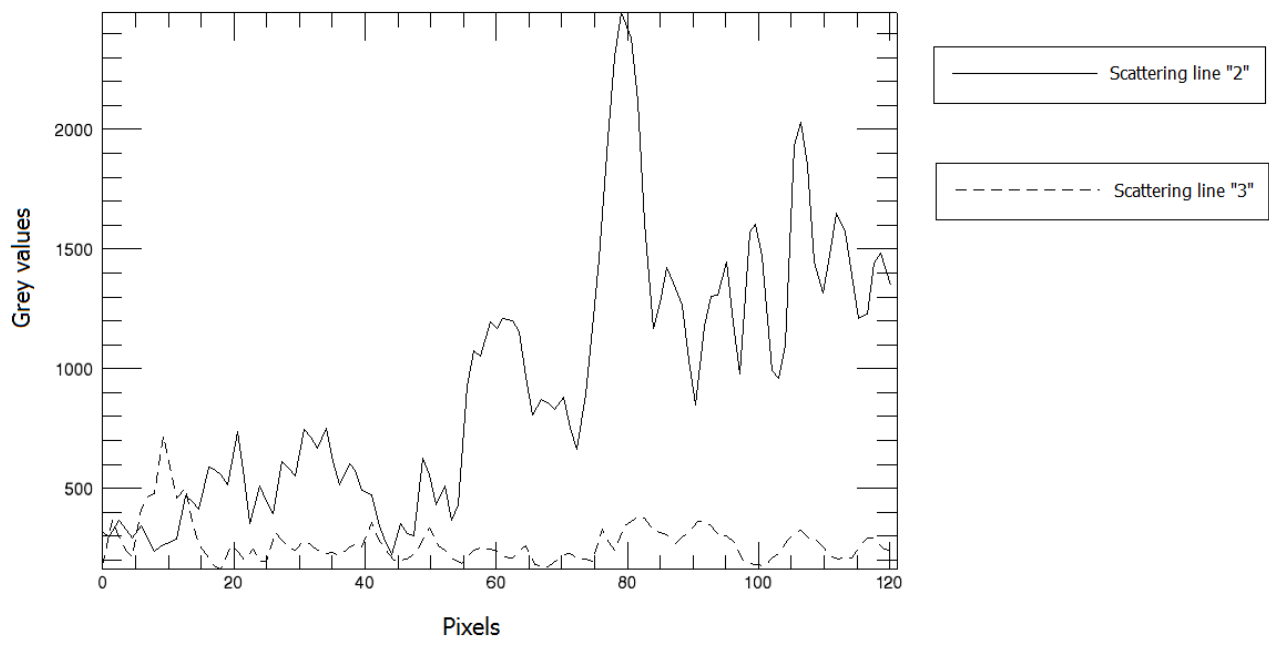
Figure 6

Figure 7

Figure 8

Figure 9

Figure 10

Figure 11

Figure 12